ASME Paper Title: Performance and emission assessment of thermo-electric power plant for rotorcraft propulsion

Authors: Ioannis Roumeliotis, Francesco Arena, Yize Liu, Stavros Vouros, Vassilios Pachidis, Olivier Broca, Djiby Toure, Deniz Unlu

ASME Conf Title: ASME Turbo Expo 2020

Volume/Issue: _Volume 5_____ Date of Publication (VOR* Online) _11 January 2021____

ASME Digital Collection URL: https://asmedigitalcollection.asme.org/GT/proceedings/GT2020/84140/Virtual,%20Online/1094886

DOI: https://doi.org/10.1115/GT2020-15724

ASME Turbo Expo 2020: Turbomachinery Technical Conference and Exposition
September 21-25, 2020, Virtual, Online, GT2020-15724
DOI:10.1115/GT2020-15724

PERFORMANCE AND EMISSION ASSESSMENT OF THERMO-ELECTRIC POWER PLANT FOR ROTORCRAFT PROPULSION

Ioannis Roumeliotis, Francesco Arena
Cranfield University, UK
i.roumeliotis@cranfield.ac.uk,
francescoarena94@outlook.com

Yize Liu, Stavros Vouros, Vassilios Pachidis
Cranfield University, UK
yizeliu.liu@cranfield.ac.uk, s.vouros@cranfield.ac.uk,
v.pachidis@cranfield.ac.uk

Olivier Broca, Djiby Toure, Deniz Unlu
Siemens Industry Software, France
olivier.broca@siemens.com, djiby.toure@siemens.com,
deniz.unlu@siemens.com

ABSTRACT

This paper assesses a gas turbine based parallel rotorcraft hybrid electric propulsion system in terms of overall performance and emissions. Three different electric power train technology levels and three different power management strategies are considered for identifying the potential benefits of hybridization in relation to technology advancements and quantifying the effect of PMS. For this analysis, a Passenger Air Transport of a twin-engine medium helicopter is used.

The propulsion systems mission simulation and emissions calculation are performed in Simcenter Amesim. The assessment framework integrates a thermal power-plant model, an electric power plant model for the hybrid electric cases, a helicopter simulation model and suitable pollutant emissions calculation correlations.

For establishing NO_x emission correlations that can be used for turboshaft engine calculations, a systematic evaluation of different correlations available in the literature is performed. The correlations are compared for different operating points against a calibrated stirred reactor model. The suitable correlations are utilized in the framework. The propulsion system is sized according to the technology levels and power management strategy considered, updating the helicopter Take-Off Weight for each case.

The results indicate that there is potential for efficiency betterment and CO_2 emissions reduction. The benefits strongly depend on the power management strategy and energy and power density of the electric power train. For current technology level and for the cases examined herein no benefits in terms of overall performance and emissions accrue. If future technology level is considered, hybridization may offer benefits in terms of performance to the expense of NO_x emissions for the case that the power train is used for boosting and the gas turbine is scaled down. Power splitting may offer block fuel, turbine life and NO_x benefits to the expense of overall energy performance.

INTRODUCTION

The conventional rotorcraft, or helicopter, emerged in the first 30 years of the 20th century. Since then it has demonstrated its diversity and versatility. Rotorcraft operations are performed worldwide in different industries, for various purposes and in order to accommodate a plethora of services. It is a typical vehicle for missions such as emergency medical and rescue, surveillance and agricultural inspection. Rotorcraft also support ferrying personnel and equipment to and from oil and gas installations and offshore wind farm, while the transport/air taxi missions, which have been a marginal activity until now, is expected to boom in the near future [1].

Conventional rotorcraft has significantly improved over the years in terms of performance and environmental effectiveness but technological growth and evolution of modern societies has created a demand for cleaner and faster transportation of people and goods. This societal demand has been quantified by the Advisory Council for Aeronautics Research in Europe (ACARE) in its Strategic Research and Innovation Agenda (SRIA) for the future. One of the key goals is the protection of the environment and the energy supply, aiming for a 75% reduction in CO_2 emissions per passenger kilometre and a 90% reduction in NO_x emissions for year 2050.

In this context, improving the energy efficiency of conventional rotorcraft without limiting their utility is a necessity and becomes even more important given the forecasts that the helicopter market will increase from an existing ~25,000, to ~37,000 helicopters by 2036 [2]. Additionally, the overall emissions of new configurations should be assessed establishing that energy efficiency is followed by lower NO_x emissions.

As discuss by Danis et al [3], transitioning to hybrid-electric propulsion can benefit rotary-wing aircraft. Thermo-electric configurations bring a certain level of flexibility into the powerplant design and the vehicle as a whole, potentially making it more energy efficient. Electrical technology can enable variable rotor speed, by decoupling the gas turbine rotational speed from the rotor one, which may reduce the main rotor power requirement up to 14% across different flight phases as discussed by Mistry and Gandhi [4]. Additionally, electrification can enable better throttle response, given the almost instant high torque capability of electric components [5], it may enhance energy harvesting and reduce the need for heavy gearboxes [3]. These advantages come with increased

weight and complexity of the whole propulsion system, thus for assessing the performance of a hybrid propulsion system the increased weight of the helicopter should be considered.

Concerning emissions, NO_x emissions of rotorcraft gas turbine based hybrid electric propulsion (HEP) systems have not been assessed since there is limited information available for turboshaft engines. The main source is the Swiss Federal Office of Civil Aviation (FOCA) database [7], which has been used to produce a correlation of NO_x emission in relation to engine shaft power. However, a correlation utilizing shaft power for evaluating NO_x emissions has specific limitations especially when aspects such as engine scaling and advanced cycles are considered. For example, in the case of a downscaled engine, the nominal power is reduced but the engine may operate more time at higher combustor temperature, promoting NO_x formation. For this reason, in order to evaluate NO_x emissions in a consistent way a systematic assessment of NO_x correlations available in the literature is performed. The ones that can provide consistent results for the turboshaft engine used herein are identified. The correlation methods are evaluated against FOCA values, which provide upper and lower values, and against a validated stirred reactor model.

The aim of this paper is to assess both performance and emissions for a parallel hybrid configuration for a Twin Engine Medium (TEM) Helicopter. For this purpose, an integrated model is developed in Simcenter Amesim [8]. The integrated model includes the helicopter model, the propulsion system model (conventional and hybrid) for calculating energy consumption and the correlations for emission calculation. In this way, the effect of propulsion system weight on overall performance and emissions can be directly evaluated along with the sub-systems performance and operability.

The introduction of thermo-electric powerplant for TEM rotorcraft propulsion depends on the development of innovative commercial technologies for increasing electric motors and batteries power and energy density respectively. In this work three technology levels are considered, one labelled as current technology, one plausible in the future and one future optimistic for identifying the potential benefits of hybridization in relation to technology advancements.

Additionally to the level of technology, it is of importance to utilize the flexibility that hybridization brings to the propulsion system. In this context Power and Energy Management Strategies (PMS) are critical for establishing the potential benefits of HEP systems. For quantifying the PMS effect on performance and emissions in correlation to technology level three different PMS are applied.

For the first PMS the electric powertrain is the sole power source during take-off (T/O) climb and descent, while the gas turbine is used during cruise for providing propulsion power and for charging the batteries. This PMS may be interesting for reducing brownout effect on the engine and pollutant emission close to the airfield. For the second PMS the electric power train is used for boosting the thermal engine throughout the mission, while the gas turbine has been scaled down. The electric power train is sized based on the energy and power needed to satisfy the engine ratings in terms of both power and duration (energy). This PMS is expected to shift the gas turbine operation to more favourable operating points in terms of efficiency. The third PMS assessed herein is based on power split, where the electric power train provides a specific percentage of propulsive power throughout the mission accomplishing a kind of active engine derating for reducing NO_x emissions and increasing engine life.

Having established a suitable simulation and analysis framework the different power management strategies are assessed for different hybridization and technology levels and the benefits and penalties accrued from utilizing hybrid propulsion are assessed and discussed, highlighting the importance of PMS applied on performance and emissions.

INTEGRATED PROPULSION SYSTEM MODEL

An integrated propulsion system model has been developed for assessing elements of rotorcraft hybridization. The integrated model includes the helicopter model, the propulsion system model (conventional and hybrid) and the correlations for emission calculation. These models and correlations are described herein.

Helicopter Model

A UH-60 helicopter performance model is developed for the prediction of total power requirements along a designated mission scenario. The main rotor model is based on a blade-element-type discretization, comprising a steady and linear inflow model [9], coupled with a steady, non-linear airfoil aerodynamic representation. For the special case of hovering flight, a combined blade element momentum theory approach is employed for the evaluation of axisymmetric rotor inflow [10]. A rigid rotor blade representation is adopted which complies with the fidelity required for steady performance evaluations [11]. Tail rotor power is estimated as a fraction of main rotor power based on the semi-empirical method provided in [10]. Fuselage aerodynamic forces and moments are calculated based on look-up tables retrieved from [12]. The integrated models are deployed within a longitudinal trim algorithm implemented via the Powell hybrid method [13] solving for main rotor collective and longitudinal cyclic pitch control angles and fuselage pitch attitude. Figure 1 presents a comparison of the predicted main rotor power coefficient against published flight test data for a range of cruise advance ratios and for a weight coefficient Cw=0.0065 [14]. As seen very good agreement is observed between predicted and measured performance data, which demonstrates the applicability of the model in the context of mission performance evaluation.

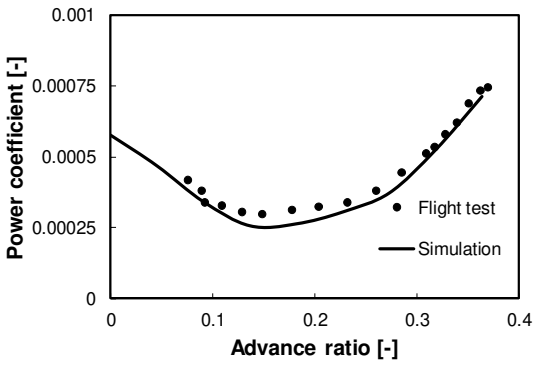

Figure 1: Main rotor power requirement for a range of advance ratios at Cw=0.0065 [-]; comparison with flight test data retrieved from [14].

The helicopter model is used for providing the torque and rotor rotational speed to the propulsion system, hence shaft power. During the mission simulation the fuel consumption is fed back to the helicopter model for performing rotorcraft all-up mass (AUM) calculations.

Propulsion System

Two propulsion system are considered herein, a conventional gas turbine and a parallel HEP gas turbine based. Two relevant models have been developed in Simcenter Amesim system simulation platform utilizing the gas turbine library [15] and the electric component libraries ([16], [17]), the HEP configuration is depicted in Figure 2. The gas turbine conventional configuration acts as the baseline. A basic control system is in place for the propulsion system, for both, conventional and HEP configurations. The thermal – electric power split for the HEP system depends on the PMS applied. The fuel flow acts as the gas turbine setting parameter for matching the power demanded from the thermal power train. The maximum continuous rating (MCR) turbine entry temperature (TET), acts as a limiter for the gas turbine controller. The fuel consumption is fed to the helicopter model for updating the vehicle weight and consequently the propulsive power for each operating point.

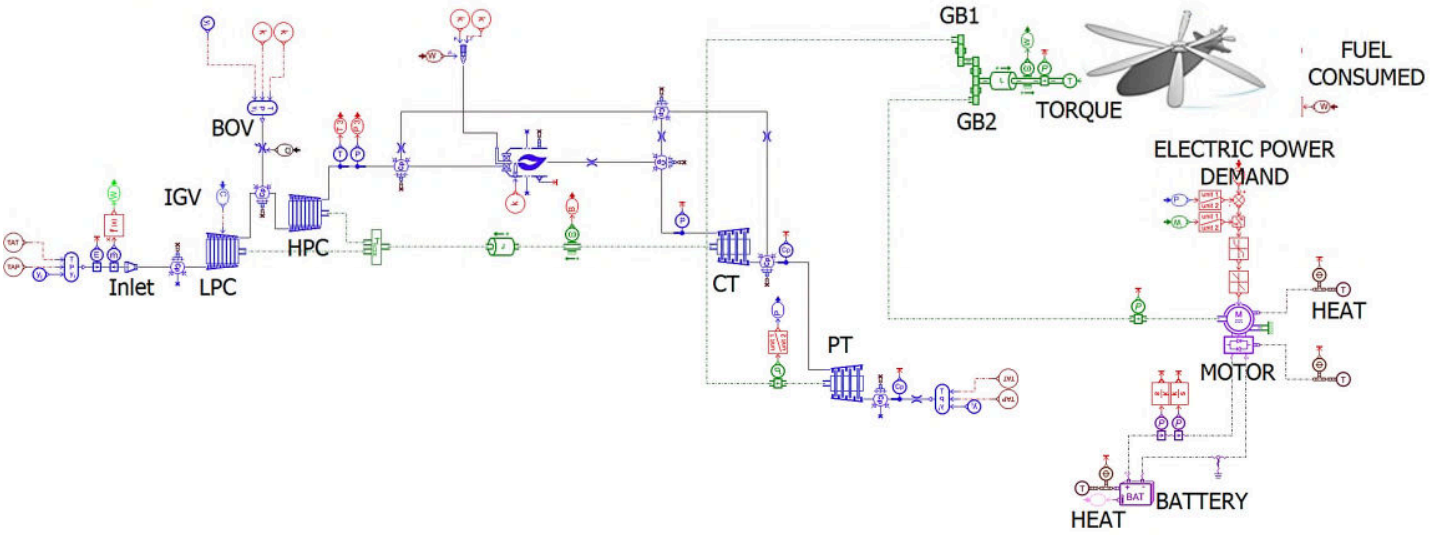

Figure 2: Gas Turbine based HEP parallel configuration model architecture

Gas Turbine

The gas turbine engine model is based on the T700-GE-700, a two-shaft turboshaft engine broadly used in TEM helicopters. It consists of a five-stage axial and a single-stage centrifugal flow compressor mounted on the same shaft; a low-fuel-pressure, annular combustion chamber; a two-stage axial flow gas generator turbine; and a two-stage uncooled independent power turbine [18]. A model capable to represent with very good accuracy the steady state and transient operation of the engine has been developed by the authors [5] and validated against data reported by Ballin [19].

The model is capable of simulating the engine whole operating envelope down to idle. For establishing low power operation, the component maps are extrapolated following the method suggested by Gaudet and Gauthier [20]. For low load operation, the low pressure

compressor utilizes variable geometry vanes (VGVs). The variable geometry effect on turbomachinery map is simulated by applying the simplified methodology described by Kurzke [21] assuming no effect on efficiency as suggested by Roumeliotis et al. [22]. Additionally for gas generator corrected rotational speed lower than 87%, which corresponds to approximately 250kW of power a bleed off valve (BOV) positioned between the axial and centrifugal compressor starts opening. The BOV is modelled as a variable area orifice. The engine performance is depicted in Figure 3.

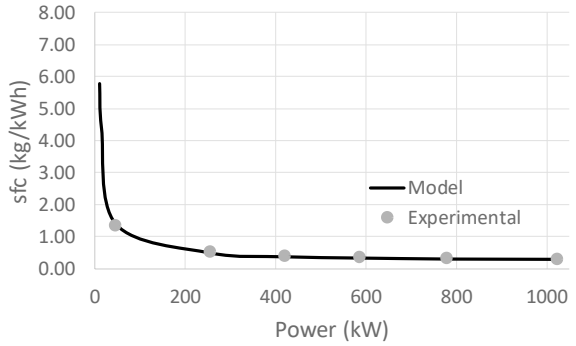

Figure 3: Gas turbine performance, experimental values from [19]

The compressors operating lines for steady state operation are depicted in Figure 4 for the axial low-pressure compressor and in Figure 5 for the centrifugal high-pressure compressor.

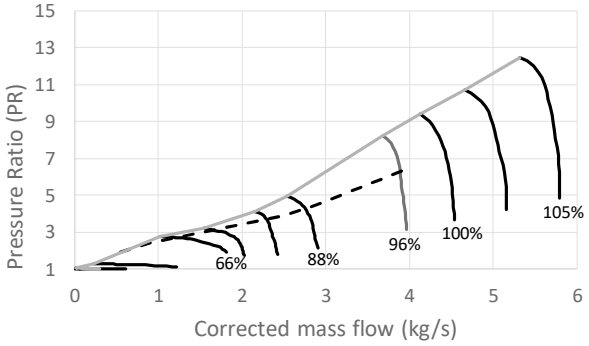

Figure 4: Axial compressor operating line

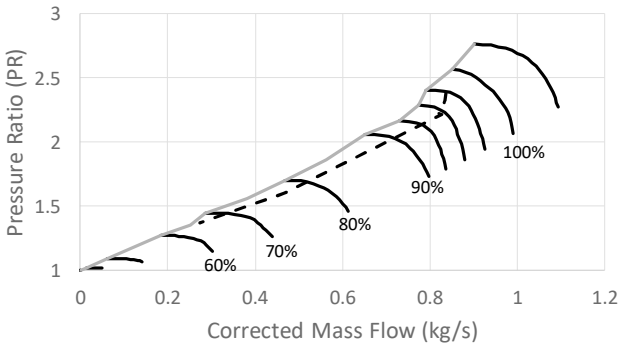

Figure 5: Centrifugal compressor operating line

An important aspect in multi-disciplinary calculations is the systems weight. The gas turbine weight and size are calculated using the Cranfield University in-house software named ATLAS [23]. ATLAS has been used for turboshaft and turbofan engines weight and flow path estimation providing results in very good agreement with available data as seen for the case of turboshaft engines in

Table **1**. In this work ATLAS is used to calculate the gas turbine weight when cycle resizing is considered.

Table 1: Turboshaft engines weight estimation with ATLAS [5], [24]

ENGINE	ATLAS	DATA [18]	Δ [%]
CT78-A	250.5	243.6	2.8
Makila 1A1	256	241	6.2
T700-GE-700	186	198	5.9

Electric Power Train

The electric power train is modelled utilizing the available low fidelity models of Simcenter Amesim for easy scaling and for reducing the data needed. The motor is simulated using a functional model of an electric drive system (machine, inverter, sensor and control unit). The motor part load efficiency is calculated applying the procedure reported in [25]. The losses (armature, core, friction and stray) are derived as a function of power. The overall efficiency is calculated through eq. (1). Figure 6 exemplify typical losses for 100kW electric motors over its whole operating range for constant rotational speed.

$$\eta_m = \frac{P_m}{P_m + \sum_i P_{loss_i}} \qquad (1)$$

The inverter part load efficiency is calculated following the component losses approach. The diode and Insulated Gate Bipolar Transistors (IGBT) losses (switching and conduction) are considered mainly a function of current and are calculated according to [26]. The inverter part load efficiency as calculated in good agreement with available data, as seen in Figure 7, giving an error in the range of ±1.3%, which is considered acceptable.

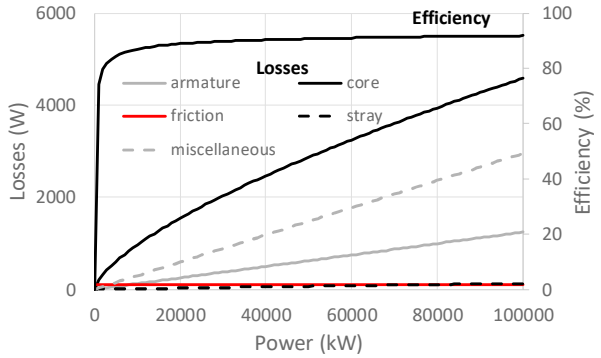

Figure 6: Power losses for a 100kW, 3600 rpm motor

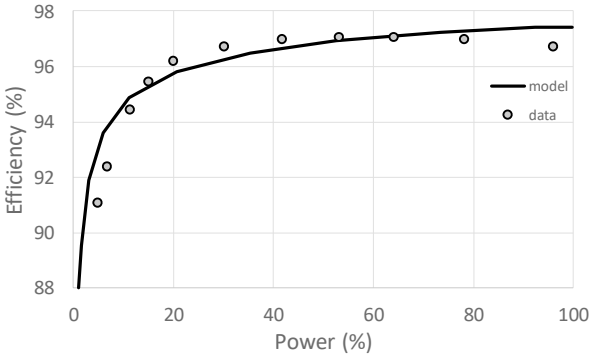

Figure 7: 285 kW - 455V inverter efficiency calculated values vs available data [29]

The batteries are modelled by applying the simplest equivalent circuit model of Simcenter Amesim as depicted in Figure 8. In this model the open circuit voltage (OCV) and the ohmic resistance (R) define the battery performance. These values and their variation with SOC (State of Charge) and temperature are derived through the battery sizing. The battery sizing is done according to [27] and [28] utilizing the software sizing tool. For specific battery type and nominal energy, power and voltage requirements, the battery OCV and charge and discharge resistance are estimated. The curves of these performance parameters as a function of SOC and temperature are

populated utilizing .publicly available data, as seen in Figure 9. The OCV defines the battery voltage when it is at rest and the ohmic resistance defines the instantaneous voltage drop depending on the charge or discharge current.

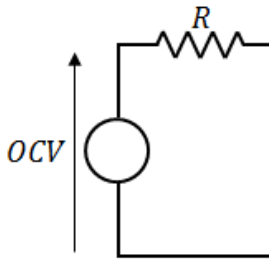

Figure 8: Battery equivalent circuit

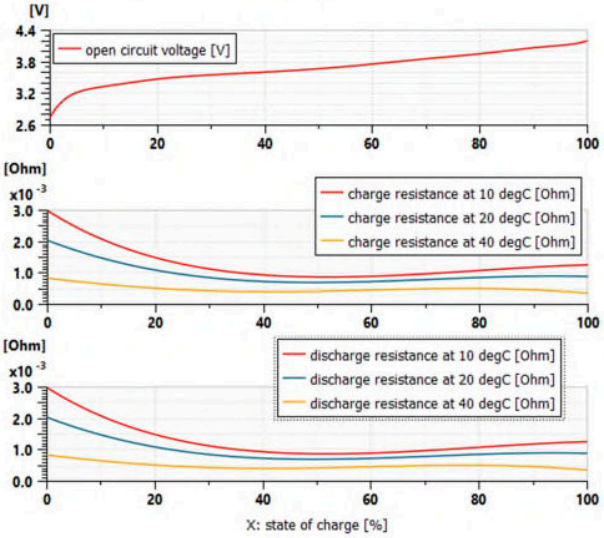

Figure 9: NCA (Lithium nickel cobalt aluminum oxide battery) battery performance parameters for nominal power of 280kW, energy 100kWh and 580V [8]

The electric power train weight is estimated by calculating the weight of each component. These calculations have been added to the ATLAS framework. For batteries and inverter, the simplified approach of energy and power density is used, as discussed in [5]. For the motor and generator, the method suggested in [25] is used (Figure 10) using data reported in [30]. The design variables are the design and maximum power and rotational speed, the number of phases and number of poles. The material properties library is populated using data from [30] and [31]. Following, the electric machine components (stator, rotor, shaft and armature) size and weight are calculated. The overall mass is obtained summing the component weights. A service mass equal to 13% of the total is added to take into account the added weight of cables and mountings as suggested in [32]. The weight estimation method has been validated against motor and generator data available in the literature. The method gives acceptable results in terms of total weight for the power ranges expected herein, as seen in Table 2.

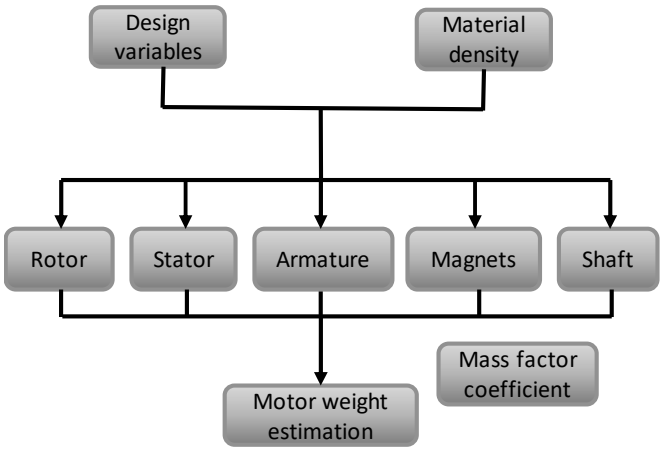

Figure 10: Motor weight calculation workflow

Table 2: Motor weight estimation

MOTOR TYPE	MODEL	DATA	Δ [%]
40kW PMS [33]	19.1	18.9	1.37
250kW MARINE GEN @ 1050rpm [30]	293	283.3	3.42
22.2MW HTS [25]	1255	1100	14.1

Emissions Prediction

There are many correlations, which can be used to estimate NO_x emissions for given operating conditions. However, they often yield very different results, even though the engine parameters remain the same. This is because these correlations are usually derived for specific engines or engine families. When such experimental data are available, correlations found in the literature can be corrected with certain coefficients in order to fit the measurements, as discussed by Tsalavoutas et al. [34]. In the case of helicopter engines, the only available data are provided by FOCA [7]. In particular, FOCA reports both the measurements which were taken by the Swiss office itself and those provided by the DLR Institute of Combustion Technology. These measurements are correlated with the engine power.

However, this approach is not suitable for predicting NO_x emissions when an engine is scaled down or when advanced cycles are considered (e.g. recuperated). For the case of downsized engines, the shaft power is reduced but depending on the mission, the engine may operate at higher temperatures promoting NO_x formation. Similarly, a recuperated engine produces less power not due to combustor primary zone temperature decrease but due to the heat exchanger pressure losses.

In this context, for assessing scaled down engines due to hybridization, correlations for evaluating rotorcraft engine NO_x emissions based on thermodynamic properties should be identified. Since correlations for this kind of engines are not available in the literature, a systematic analysis of correlations used in aviation is performed. The aim is to establish the ones that can provide acceptable results for the type of engine considered. The correlations are compared against a stirred reactor model. Additionally, the lower and upper values reported by FOCA are used as boundaries. The correlations that produce results in between the FOCA limits following physical consistent trends compared to the stirred reactor model are considered as suitable for NO_x calculations in this study.

Stirred Reactor Method

The stirred reactor method modelling process is composed of a number of steps:

- the combustor inlet thermodynamic parameters (P3,T3,W3), air and fuel are input from the engine performance model;
- the combustor under investigation is divided into a number of zones based on the layout/configuration of the combustor (i.e. flame front primary zone, intermediate zone and dilution zone.) and the relevant geometry;
- within each zone, the type of stirred reactor is chosen based on the gross flow features;
- a network is established to enable the chemical reaction taking place along the combustor for obtaining the emission index (EI), temperature and species concentration along the combustor

The details of the reactor network used herein are depicted in Figure 11.

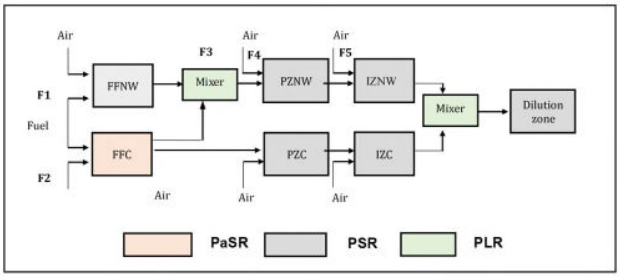

Figure 11: The reactor network arrangement for emission prediction for T700-GE-700 model

The first part of the combustor primary zone, which simulates the initial mixing and reaction of the fuel with the nozzle and air swirler – called flame front (FF), is modelled using a partially-stirred reactor (PaSR). It considers inhomogeneities in this combustor region. The downstream zones (Primary zone PZ, intermediate zone IZ and dilution zone DZ) are modelled by Perfectly Stirred Reactor (PSR) considering the fuel-air mixing is enhanced. Near wall reactors are created to simulate the emission closed to the wall. Plug flow reactor is also employed to simulate the two-stream mixing process. In this case, one mixer is used to simulate the fractional burning gas admitted into the primary zone near wall reactor, the other mixer is used to simulate the mixing between the core and near wall reactor before reaching dilution zone.

The kinetics models are incorporated in each reactor to predict the formation rate of pollutants. In this case, the formation rate of thermal NO_x is determined using the following equation reported by Celis [35], which takes into consideration N_2O contribution to NO formation as well:

$$\frac{dY_{NO}}{dt} = \frac{2\bar{M}_{NO}}{\rho}(1-\alpha^2)\left\{\frac{R_1}{1+\alpha K_1}+\frac{R_6}{1+K_2}\right\} \qquad (2)$$

Where R_i denotes a 'one-way equilibrium' reaction rate, K_1 and K_2 are reaction rate coefficients and α is NO concentration ratio. The prompt NO_x formation rate is evaluated using the De Soete's model [36]:

$$\frac{\mathrm{dY_{NO}}}{\mathrm{dt}} = \left(\frac{\bar{\mathrm{M}}_{\mathrm{NO}}}{\rho}\right)\mathrm{f_{pr}k'_{pr}([O_2]_e)^a[N_2]_e[C_{12}H_{23}]}\cdot \exp\left(\frac{-36499.507}{\mathrm{T}}\right) \qquad (3)$$

Where

$$\mathrm{f_{pr}} = 4.75 + 0.0819\mathrm{x} - 23.2\emptyset + 32\emptyset^2 - 12.2\emptyset^3$$

$$\mathrm{k'_{pr}} = 6.4\times10^6\left(\frac{0.0820575\mathrm{T}}{\mathrm{P}}\right)^{\mathrm{a+1}}$$

$\mathrm{f_{pr}}$: correction factor that incorporates the effect of fuel type,
a: a function of the oxygen mole fraction ($\mathrm{X_{O_2}}$),
x: number of carbon atoms per fuel molecule
$\emptyset$: is the equivalence ratio in the reactor

Based on the concentration of oxygen mole fraction $\mathrm{X_{O_2}}$, the relationship between a and $\mathrm{X_{O_2}}$ is shown below:

$$\begin{cases} 1.0, & \mathrm{X_{O_2}} \le 4.1\times10^{-3} \\ -3.95 - 0.9\ln \mathrm{X_{O_2}}, & 4.1\times10^{-3} < \mathrm{X_{O_2}} \le 1.11\times10^{-2} \\ -0.35 - 0.1\ln \mathrm{X_{O_2}}, & 1.11\times10^{-2} < \mathrm{X_{O_2}} \le 0.03 \\ 0.0, & \mathrm{X_{O_2}} \ge 0.03 \end{cases}$$

The overall mass of NO formed within each reactor can be calculated by integrating the formation rates with respect to the corresponding residence times and then summing the two values. The reactor models have been validated for different combustors including single annular and double annular combustors ([37], [38])

Emission Correlations

There is a plethora of correlations for gas turbine NO_x prediction in the literature for different combustor types. Lefebvre and Ballal [39] provide an excellent insight on semi-empirical correlations, Tsalavoutas et al. [34] evaluated several correlations suitable for NO_x prediction from cycle data for conventional combustors while Kyprianidis et al. [40] presented an adaptable NO_x emissions correlation for modern and future RQL (Rich Burn, Quick Mix, Lean Burn) combustors. A systematic analysis of 15 correlations, reported in Table 3 has been performed for identifying the ones that give results in the expected range, in-between FOCA band and in agreement with the stirred reactor model. Five of these correlations give results within the FOCA band and are in good agreement with the stirred reactor method trend without the need of calibration, as seen in Figure 12. The performance data of the T700-GE-700 model for different operating points is used for calculating the correlations parameters.

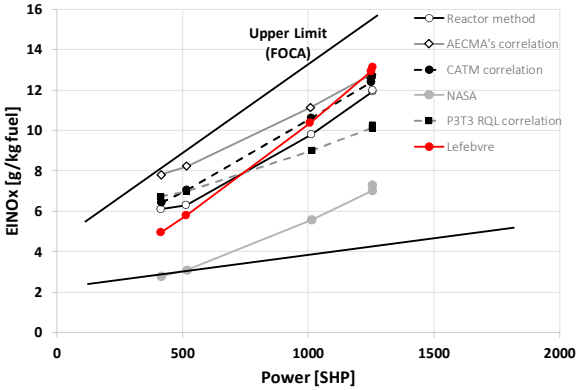

Figure 12: EI NO_x prediction for different power settings of the T700-GE-700 model

Table 3: Equations assessed for rotorcraft NOx emissions

Name	Ref	Inside FOCA band	
		Yes	No
European Association of Aerospace Industries (AECMA)	[41]	X	
Becker et al.	[42]		X
Blazowski	[43]		X
Committee of Aeronautical Technologies Method (CATM)	[44]	X	
Lefebvre	[39]	X	
Lewis	[39]		X
Lipfert	[44]		X
NASA	[44]	X	
Numerical Propulsion System Simulation (NPSS)	[44]		X
Odgers and Kretschmer	[39]		X
P3T3 correlations for LDI combustors	[45]		X
P3T3 correlations for RQL combustors	[40]	X	
Perkavec	[42]		X
Rizk and Mongia	[39]		X
Rokke et al.	[39]		X

It should be noted that the NASA correlation is derived for a lean direct injection (LDI) combustor using multi-point injection hence the absolute values of NO_x calculated are less than the ones derived for conventional combustors. AECMA and CATM correlations developed based on conventional combustors are in good agreement with Lefebvre correlation and the stirred reactor model results. Concerning the P3T3 RQL correlation, it presents a smaller gradient over higher power – higher TET compared to other correlations,

which can be justified by the combustor technology. Given the above, the Lefebvre (conventional), NASA (LDI) and P3T3 RQL correlations are used in this study for assessing the NO_x emissions of the propulsion systems.

European Association of Aerospace Industries (AECMA) [41]

$$EI_{NOx} = 2 + 28.5\sqrt{\frac{P_3}{3100}}exp\left(\frac{T_3 - 825}{250}\right) \quad (4)$$

Committee of Aeronautical Technologies Method (CATM) [44]

$$EI_{NOx} = 32\left(\frac{P_3}{2965}\right)^{0.4} \cdot exp\left(\frac{T_{03} - 826}{194} + \frac{6.29 - 100h_{alt}}{53.2}\right) \quad (5)$$

NASA [44]

$$EI_{NOx} = 33.2\left(\frac{P_3}{432.7}\right) \cdot exp\left(\frac{T_3 - 459.67 - 1027.6}{349.9} + \frac{6.29 - 6.3}{53.2}\right) \quad (6)$$

P3T3 for RQL [40]

$$EI_{NOx} = \left(8.4 + 0.0209\, e^{(0.0082\, T_3)}\right)\left(\frac{P_3}{3000}\right)^{0.4} \cdot \exp\left(19\,(0.006344 - h)\right) \quad (7)$$

Lefebvre [39]

$$EI_{NOx} = \frac{9 * 10^{-8} {P_3}^{1.25} V_{pz} e^{0.01\, T_{st}}}{W_A T_{pz}} \quad (8)$$

T_{st}, T_{pz} are stochimetric and primary zone temperatures accordingly, V_{pz} is primary zone combustor volume and W_A is the air mass flow, while stoichiometric temperature is calculated using the method reported in [46]. The combustor volume is derived applying the 1-D combustor sizing method proposed by Murthy [47]. The combustor air partitioning is based on data and methods suggested by Melor [48], Li et al. [49] and Mattingly et al. [50]. The primary zone temperature is calculated via the gas turbine model utilizing suitable combustor modelling (splitting the combustor to primary and secondary zone) as seen in Figure 13.

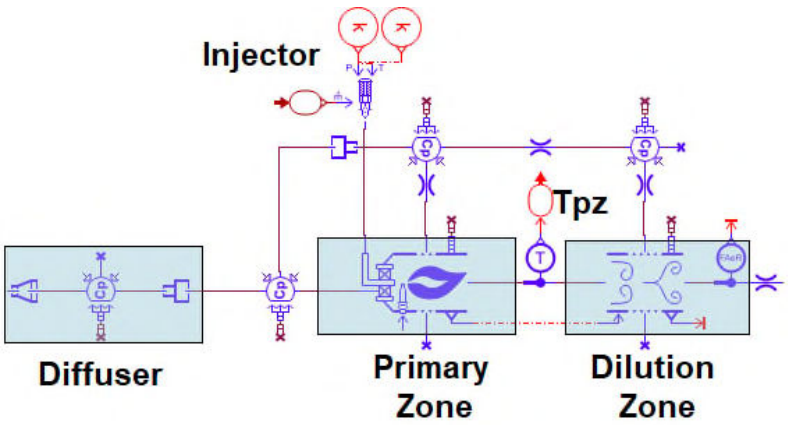

Figure 13: Gas turbine combustor model for deriving primary zone temperature

SYSTEMS ASSESSMENT

In this work, one of the aims is to identify the potential benefits of power plant hybridization for current and future electric components technologies. In this context, three technology related cases concerning electric components energy and power density are defined based on the literature data. The mission to be used for the propulsion system assessment is a Passenger Air Transport (PAT) one, an activity that is expected to develop rapidly in the near future.

Three PMS are applied. For the first one (PMS1) the electric power system is utilized for short period providing high power. Specifically, the electric power train provides all the shaft power for T/O, climb, descent and landing, with the gas turbine idling. The gas turbine provides the propulsion power and charge the batteries during cruise. For the second (PMS2), the electric system supplements the gas turbine for generating the propulsive power. In PMS2 the gas turbine is scaled down from 90% to 70% of the baseline engine. PMS2 allows the movement of the gas turbine operation towards higher specific power, hence towards higher efficiency. The third PMS assessed herein (PMS3) is based on power split, where the electric power train provides a specific percentage of propulsive power throughout the mission, accomplishing a kind of active engine derating for reducing NO_x emissions and increasing engine life.

Helicopter mission

A PAT mission is considered herein: the helicopter transports the passengers from an assumed origin to a destination located 500km far from the origin. The propulsion system operates at low power setting for 5 min prior and after the mission. The helicopter baseline Take-Off Weight (TOW) is assumed 6000kg. The mission flight and power profile are depicted in Figure 14 and Figure 15 respectively. The maximum TOW considered in this study is 8000kg.

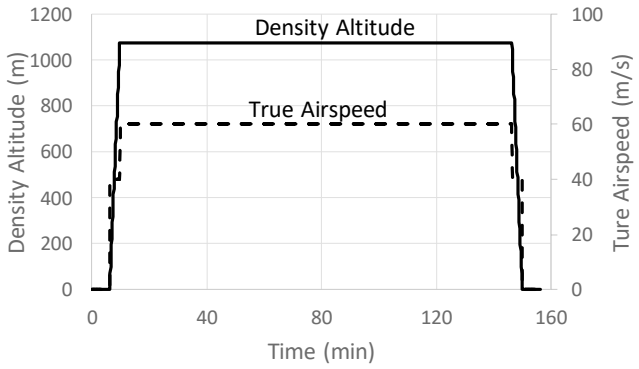

Figure 14: Mission density altitude and true airspeed flight profiles

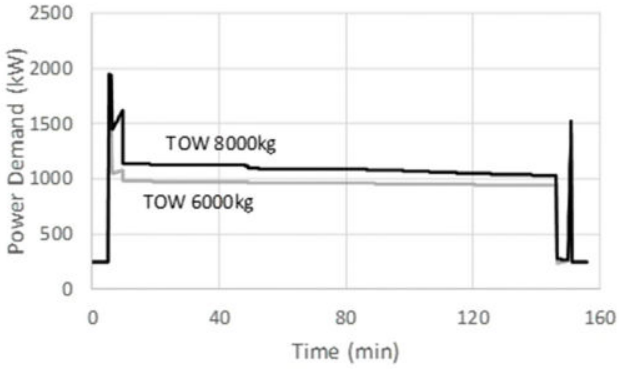

Figure 15: Mission total power requirement profile

Electric Components Technology Level

For batteries, current state-of-the art Li-ion batteries have specific energy in the range of 200 Wh/kg, while future developments are expected to increase this value up to 2000 Wh/kg [51]. The inverter power density is in the range of 2 kW/kg, while future values are expected to be as high as 16 kW/kg [52]. Inverters based on SiC material can reach 7 kW/kg [53]. Concerning the motors and generators the method described gives for current technology conventional motors a power density of about 3kW/kg, for HTS motor the power density calculated is in the range of 10kW/kg, while eAircraft presented a motor with power density in the range of 6kW/kg [54]. Based on these data three cases are considered herein, one describing current state of the art, one describing plausible future technology advancement in a time frame of +20 years and one describing optimistic future technology advancement. The relevant performance parameters are depicted in Table 4.

Table 4: Technology assumption cases

Variable	Case A	Case B	Case C
Battery specific energy [Wh/kg]	200	800	1200
Inverter specific power [kW/kg]	2	7	16
Motor power density [kW/kg][1]	3	6	10

Take-Off and Landing Fully Electric (PMS1)

For this PMS the electric motor should be capable to provide the MCR of the baseline engine during T/O and climb which is 987kW [5]. The baseline gas turbine is part of the configuration and is idling during these flight phases for redundancy. The electric power train is sized according to the following: the battery energy is calculated as the energy needed for T/O and climb to mission altitude assuming TOW of 8000kg (worst case) for the mission; which is 80kWh. As discussed by Xue et al. [55] high specific energy density leads to low specific power density, meaning that for this case the weight of the battery for providing 987kW would be significant greater than the weight calculated based on the maximum energy density value. In this context a compromise between energy and power density should be reached. The data provided by Xue et al. [55] concerning the optimal energy density vs. specific power is used for calculating an energy and power density point that provides a viable battery weight for this PMS. A new energy density of 137Wh/kg is selected. The energy density ratio of 137 over 200 is used for characterizing future technologies deriving the values seen in Table 5.

Table 5: battery specific energy for PMS1

Variable	Case A	Case B	Case C
Battery specific energy [Wh/kg]	137	548	822

The propulsion system weight is established for each technology assumption case and for each propulsion power train configuration:

- two gas turbines (baseline, 2xGT)
- one gas turbine and one gas turbine plus electric power train (1xGT and 1xGT+EL)
- two gas turbines plus electric power trains (2xGT+EL)

[1] These values are approximations since for each case the actual weight is calculated as a function of power and rotational speed

The relevant weights are presented in Table 6. The third configuration is not considered for technology Case A since the weight addition results to a TOW higher than 8000kg.

Table 6: Propulsion power train weight in kg for PMS1

Description	Case A	Case B	Case C
2xGT	372	372	372
1xGT and 1xGT+EL	1677	803	643
2xGT+EL	-	1234	915

For each case and propulsion configuration, block fuel and mission emissions are calculated. As seen in Figure 16 hybridization do not offer any benefits in terms of block fuel for the case of PMS1.

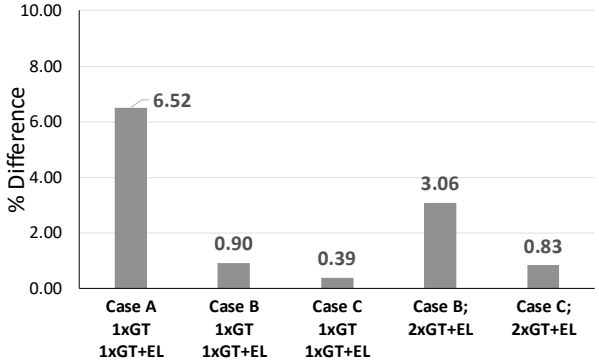

Figure 16: Block fuel change against the baseline, PMS1

As seen in Figure 17, CO_2 and H_2O emissions are proportional to the fuel flow as expected. Since the batteries are not fully charged at the end of the mission a value of $0.42kgCO_2/kWh$, suggested in [56], is applied for considering batteries recharging after landing. As seen in Figure 17 hybridization results to a significant penalty on NO_x emissions at mission level as well.

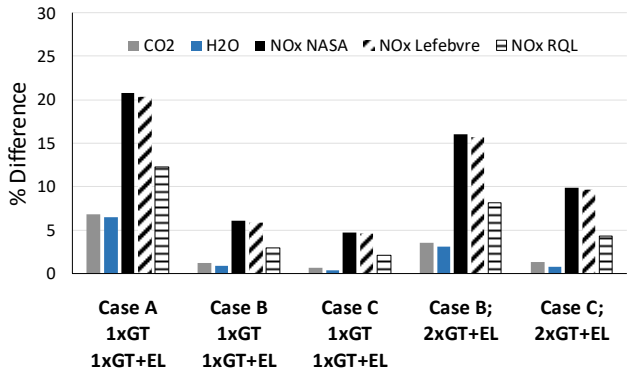

Figure 17: Pollutant emissions, PMS1

The NO_x increase is due to the engine operating at higher TET for longer periods due to battery charging after T/O and climb. If the charging rate decreases, the NO_x emissions will be reduced, albeit there is still a penalty against the baseline case. The TET variation throughout the mission for the baseline and the HEP cases for two different charging rates (fast and slow) is presented in Figure 18.

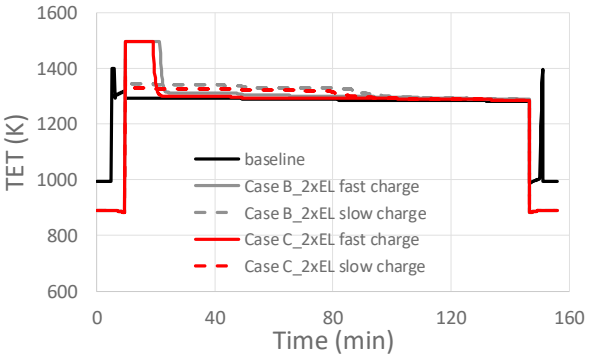

Figure 18: TET variation through the mission for different recharge rates; PMS1

The NO_x emitted mass during the mission can be seen in Figure 19 for the two recharging rates. The charge rate is expected to be a parameter for the PMS optimization, since it affects engine operation; hence emissions. It also affects the engine and battery performance; hence the overall system performance.

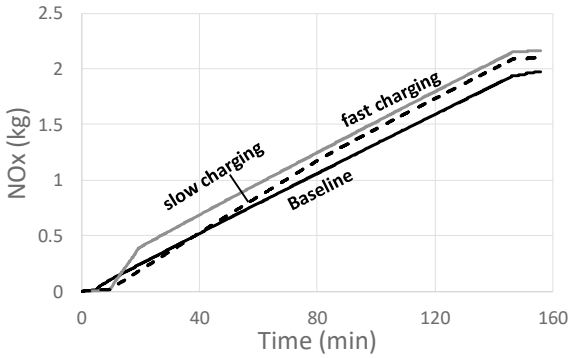

Figure 19: NO_x pollutant emissions for fast and slow recharging for Case C; PMS1

This PMS is not expected to present any benefits on performance or emissions, albeit some variations such as turning-off the gas turbine for the waiting time on ground and during descent can provide some marginal benefits when future technologies are considered, as seen in Figure 20. It can provide low emissions close to the airfields, at low altitude and give solution to brownout related engine degradation. Aspects such as thermal management may be critical for this PMS since the gas turbine is idling when the electric power train provides power, meaning that the fuel will not be efficient as a heat sink.

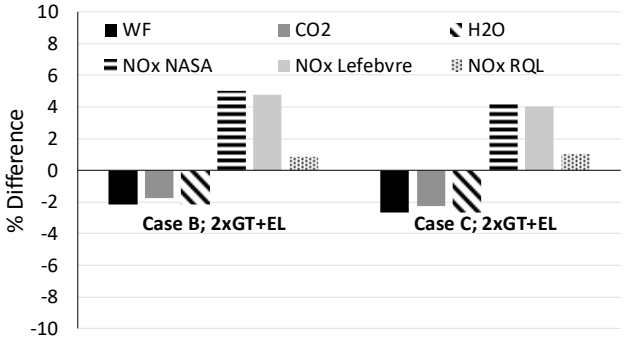

Figure 20: Performance and emissions for PMS1 for Gas Turbine off during waiting, descent, and landing

Electric Boosting PMS Assessment (PMS2)

For this PMS the prime mover is the gas turbine, while the electric power train is supporting it when more power than the designated gas turbine MCR is demanded. The gas turbine is scaled down to 90%, 80% and 70% of nominal MCR. This PMS allows the utilization of the gas turbine at high specific power-high efficiency operating points, hence it may offer performance benefits, as discussed in [5] for an Oil and Gas mission. The engine power is scaled down by scaling down the engine mass flow, reducing the engine size. The baseline engine nominal overall pressure ratio, component efficiencies and MCR turbine inlet temperature are design parameters of the scaled down engine.

The electric power train is sized for providing support to the gas turbine engine. In this context, it should, at any point, be capable to provide the surplus power, on top of the gas turbine power, for the propulsion system to achieve the OEI[2] (One Engine Inoperative) rating. This value is used for sizing the maximum power of the electric power train, depending on the engine downsizing. Additionally it should have the energy to support the gas turbine for providing the maximum intermittent rating[3] for 30 min. This value is used for sizing the battery energy. The data used herein for sizing are presented in Table 7 and are calculated for TOW of 8000kg.

Table 7: Power and energy demand used for the electric system sizing

GT Size (%)	GT MCR (kW)	Power (kW)	Energy (kWh)
100	987	0	0
90	888	121	60.5
80	790	242	121
70	691	363	181.5

The configurations examined are:

- two gas turbines (baseline, 2xGT)
- two gas turbines plus electric power trains (2xGT+EL); the gas turbines are scaled down from 0.9 to 0.7 of the baseline engine power

As in the case of PMS1 suitable energy and power density values are derived from the relation between specific energy and power provided by Xue et al. [55]. The values that offer a compromise between energy and power density are 173Wh/kg and 500W/kg respectively, since the energy becomes more important than power. The future energy density values are derived using the ratio 173 over 200 populating Table 8**.** Having defined the configurations, the subsystem power and batteries energy the power train weights are calculated and presented in Table 9.

Table 8: Battery specific energy for PMS2

Variable	Case A	Case B	Case C
Battery specific energy [Wh/kg]	173	692	1038

Table 9: Propulsion power train weight in kg

Description	Case A	Case B	Case C
2xGT	372	372	372
2xGTx0.9+EL	1390	633	531
2xGTx0.8+EL	2409	897	691
2xGTx0.7+EL	-	1162	854

As seen Figure 21**,** using current technology (Case A) PMS2 offers no performance or emission benefits. Additionally, since the scaled down engine operates at higher TET the NO_x emissions increase significantly. For Case B, the HEP configuration starts to present some benefits in terms of block fuel, but still NO_x emissions are significantly higher than the baseline ones, as seen in Figure 22.

[2] The One-Engine-Inoperative (OEI) rating powers provide rotorcraft with higher than takeoff and maximum continuous rating powers during takeoff, cruise, and landing when one or more engines of a multi-engine rotorcraft fails or is shutdown.

[3] Intermittent or Intermediate rating power of a helicopter engine is defined between one engine inoperative and maximum continuous rating power typically time-limited to 30 or 60 min.

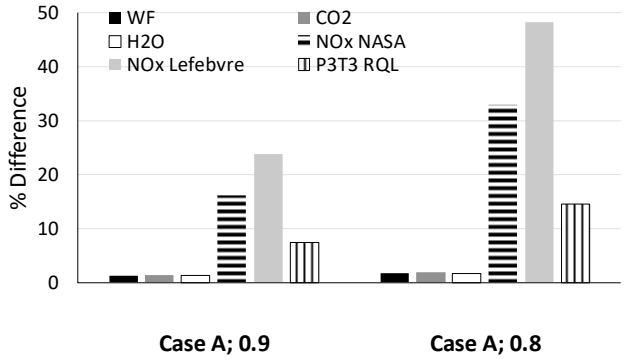

Figure 21: Block fuel and emissions change against the baseline for Case A; PMS2

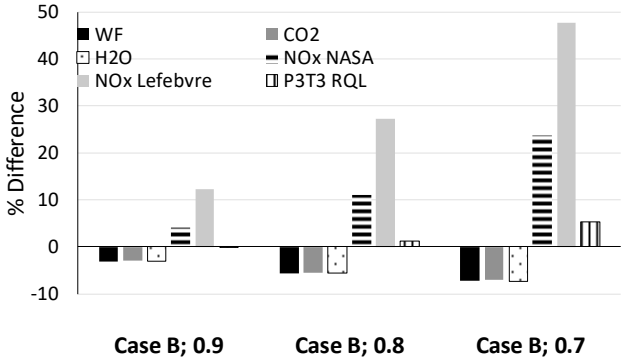

Figure 22: Block fuel and emissions change against the baseline for Case B; PMS2

Case C results indicate that a benefit in the range of 10% in block fuel may accrue, albeit there is still a significant penalty in NO_x. The P3T3 RQL method evaluates very small penalties in NO_x for Case C, indicating that modern combustor technology may keep NO_x values under control for these cases, albeit the ACARE targets with respect to NO_x reduction cannot be achieved with PMS2.

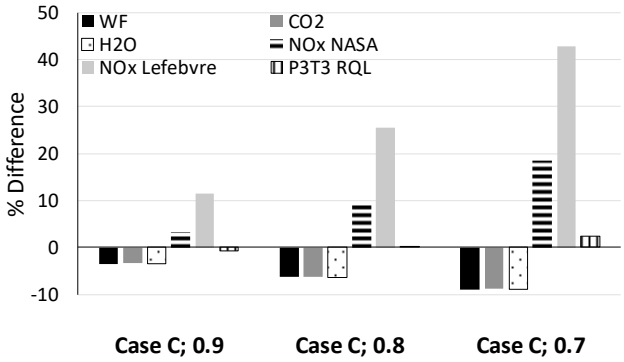

Figure 23: Block fuel and emissions change against the baseline for Case C; PMS2

As presented, there is a significant penalty in NO_x, as the engine is scaled down from the baseline. The increase in NO_x emissions is due to the scaled down engines operating at higher TET throughout the mission, as seen in Figure 24, hence at conditions that promote NO_x formation.

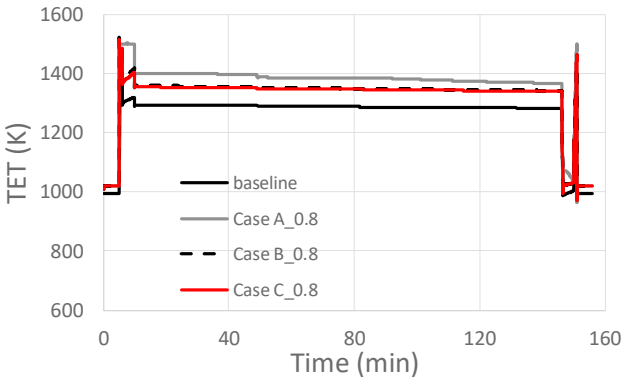

Figure 24: TET values throughout the mission, all three cases with the engine scaled down to 80% of baseline

It is interesting to note that the fuel flow reduction calculated for Case B and C cannot compensate for the engine operating point shift, hence relations correlating NO_x with fuel flow rather than operating conditions may lead to erroneous conclusions.

In the case of PMS2 the electric power train power contribution is marginal throughout the mission. It mainly acts as a booster for high power cases (T/O), so the scaled down gas turbine engine is operating at higher specific power – higher efficiency operating points. This is evident in Figure 25 where the mission overall thermal efficiency, defined according to overall mission propulsion and thermal energies (eq. (9)), is depicted.

$$eta_{th,mission} = \frac{GT\ Energy\ [kWh]}{Heat\ Input\ [kWh]} \qquad (9)$$

As seen for Case A, albeit the mission gas turbine efficiency is improved, as expected, the added weight has a significant impact on the power demand; hence, the efficiency betterment is not translated to block fuel reduction. For Case B and C the added weight is reduced and the engine efficiency benefit is translated to block fuel benefit.

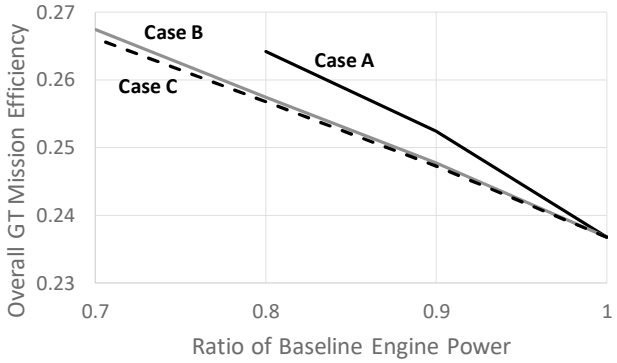

Figure 25: Overall mission gas turbine efficiency for all cases

Power Split PMS Assessment (PMS3)

For reducing the mission emissions, the gas turbine TET and fuel consumption should be decreased. PMS3 is selected for achieving pollutant emissions reductions by applying power splitting during the mission, maintaining the baseline engine. In this case, the engine operates derated at lower TET, prolonging its life and reducing NO_x formation. The PMS applied herein is: the electric power train is utilized at the waiting phases (prior to T/O and after landing), while the engine is idling. During T/O only the gas turbine operates. During cruise and descent, both power trains are used. Three cases are considered: the gas turbine provides 95%, 90% and 80% of the propulsion power. The gas turbine is the baseline one not scaled down. The electric power system is not used during descent, because the power demand is spiking thus the system would have to be significantly oversized in terms of power capability.

In this PMS, energy is critical, while the electrical power is low, so the maximum energy power density is considered as reported in Table 4. The propulsion power train weight is presented in Table 10. As before a helicopter maximum weight of 8000kg is considered, thus for Case A only the 95/5 split is examined.

Table 10: Propulsion power train weight in kg

Description	Case A	Case B	Case C
2xGT	372	372	372

2xGT (95/5 split)	1910	731	596
2xGT (90/10 split)	-	1157	865
2xGT (80/20 split)		1585	1136

As seen in Figure 26**,** PMS3 is not beneficial for the pollutant emissions or fuel consumption when current technology is considered (Case A). This change as future technologies are considered. In Figure 27 the results for Case B are depicted. The block fuel is decreased significantly, as are NO_x emissions. Gas turbine CO_2 emissions are reduced, in accordance to block fuel, but, as discussed a value of $0.42kgCO_2/kWh$ is applied for considering batteries recharging after landing. This result to a marginal increase in overall mission CO_2 (including battery recharging) for Case B, 90/10 and 80/20 power split. The results for Case C are similar. There is a significant benefit on block fuel and NO_x, while CO_2 reduces marginally. A reduction of approximately 20% of NO_x is predicted, along with a CO_2 reduction of 2%.

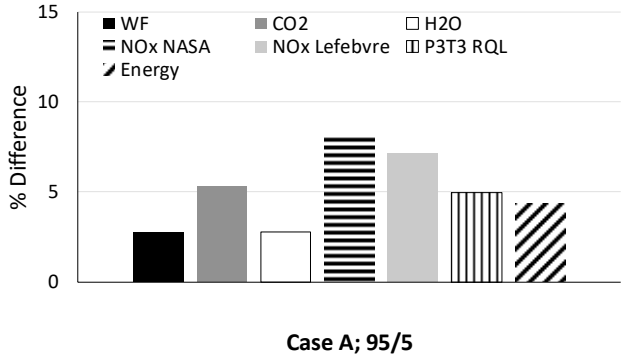

Figure 26: Block fuel and emissions change against the baseline for Case A; PMS3

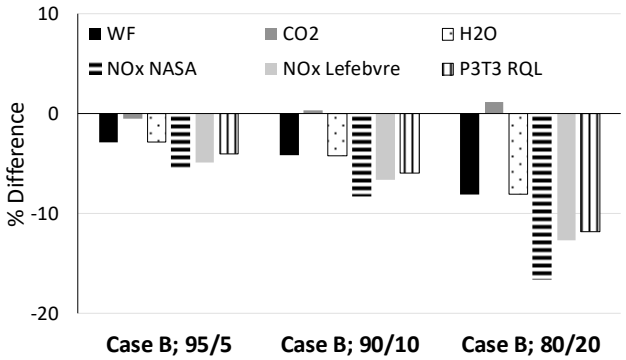

Figure 27: Block fuel and emissions change against the baseline for Case B; PMS3

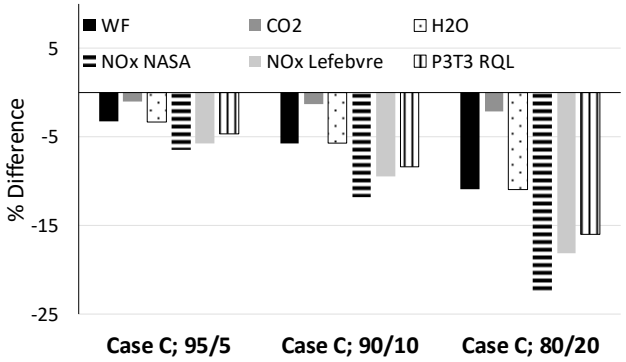

Figure 28: Block fuel and emissions change against the baseline for Case C; PMS3

From these results it can be deducted that a betterment in terms of emissions accrue for PMS3 when future technologies are considered. Additionally a benefit in turbine life is expected since the engine operates at lower TET. It should be highlighted than the block fuel reduction do not indicate a better system energy performance. The gas turbine operates at lower power setting, thus at lower thermal efficiency, as deducted from the overall mission gas turbine efficiency (Figure 29).

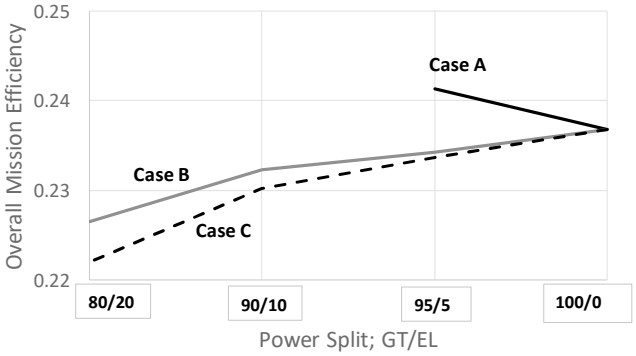

Figure 29: Overall mission gas turbine efficiency for all cases

For evaluating the system efficiency, the efficiency of the batteries charging process on land, starting from the power plant and the grid should be considered. Eq. (10) is applied considering a grid efficiency of 50%. The results indicate that for Case C the system energy efficiency can be marginally improved, especially for low hybridization values. For any other case, the system energy efficiency is reduced. It is apparent that the overall system efficiency is significantly affected by the grid efficiency. Increasing the grid efficiency, hybridization can become more appealing in terms of energy efficiency as well.

$$Sys_{cor,eff}[\%] = \frac{\text{Propulsive Energy[kWh]}}{\text{Heat Input[kWh]} + \frac{\text{Electric Energy[kWh]}}{\text{Grid Efficiency[-]}}} \cdot 100 \qquad (10)$$

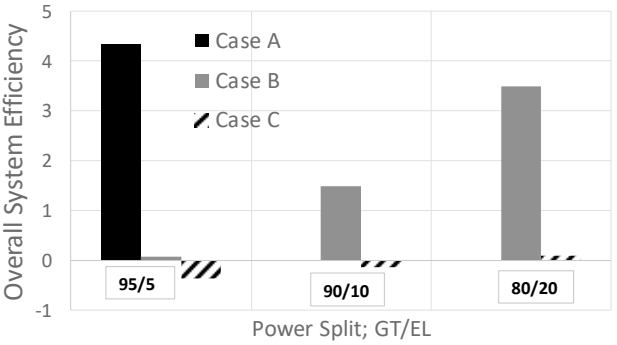

Figure 30: Overall system efficiency, assuming land charging efficiency of 50%

SUMMARY AND CONCLUSIONS

The potential benefits of hybridization for a TEM helicopter are assessed by utilizing a simulation framework developed in Simcenter Amesim. The simulation framework integrates the thermal power plant model, the electric power plant model and a helicopter model. The weight of the propulsion system is calculated for different technology levels and different PMS. The mission block fuel and NO_x emissions are calculated relative to the baseline configuration for three PMS and three technology scenarios. For performing this analysis the correlations for NO_x emission calculation that are suitable for rotorcraft application have been recognized.

The results indicate that for current technology, hybridization is not expected to bring any benefits in terms of overall performance and emissions for the three power management strategies assessed.

For future technology scenarios, PMS1 (fully electric T/O and climb) can offer some benefits in terms of near the ground pollutant emissions but not in terms of overall mission fuel consumption and pollutant emissions. The results indicate that the on-flight rate of charge should be considered since it affects engine TET; hence NO_x production.

Electric boosting (PMS2) can have some benefits in block fuel and CO_2 emissions for future technology scenarios, since the gas turbine operates at favourable operating conditions. NO_x on the other hand will increase since the scaled down gas turbine works at higher TET, hence at conditions that promote NO_x formation. For future technology scenarios (Case B and C) the benefits are in the range of 7% in terms of block fuel and CO_2 with a significant penalty in NO_x emissions.

For reducing pollutant emissions, a power splitting strategy (PMS3) can be applied. Since the engine is not scaled down, it is a way to derate it, reducing cycle high temperature, hence decreasing NO_x and turbine life consumption. This power management strategy can provide block fuel and NO_x emissions reduction, in the range of 8% and 15% respectively, when future technology scenarios are considered. The overall CO_2, emissions accounting for battery charging, only marginally decrease compared to the baseline. The overall propulsion system efficiency depends greatly on grid efficiency which characterize the efficiency for producing the electrical power used for recharging the batteries.

REFERENCES

[1] Green Rotorcraft, Clean Sky, accessed on 05/08/2018: http://www.cleansky.eu/green-rotorcraft-grc
[2] Global Helicopter Forecast, 2017, Airbus, https://www.airbus.com/content/dam/corporate-topics/publications/backgrounders/Global-Helicopter-Forecast-2017.pdf
[3] Danis R. A., Green M. W., Freeman J. L, Hall D.W., 2018, "Examining the Conceptual Design Process for Future Hybrid-Electric Rotorcraft", NASA/CR—2018–219897
[4] Mistry M., Gandhi F., 2014, "Helicopter Performance Improvement with Variable Rotor Radius and RPM", Journal of the American Helicopter Society, Volume 59, Number 4, October 2014, pp. 17-35(19)
[5] Roumeliotis I, Mourouzidis C, Zafferetti M, Deniz U, Broca O & Pachidis V (2019) Assessment of thermo-electric power plants for rotorcraft application, Journal of Engineering for Gas Turbines and Power, Available online 1 October 2019, Article No. GTP-19-1402
[6] Donateo T., Ficarella A., Spedicato L., 2018, "Applying Dynamic Programming Algorithms to the Energy management of Hybrid Electric Aircraft", ASME paper No. GT2018-76500
[7] Rindlisbacher, T. (2009). Guidance on the determination of helicopter emissions. Federal Office of Civil Aviation (FOCA), Division Aviation Policy and Strategy, Bern, Switzerland, Reference No. 0/3/2033/33-05-20
[8]https://www.plm.automation.siemens.com/global/en/products/simcenter/simcenter-amesim.html
[9] Greenwood, E., Schmitz, F. H., & Sickenberger, R. D. (2015). A semiempirical noise modeling method for helicopter maneuvering flight operations. Journal of the American Helicopter Society, 60(2), 1-13
[10] Leishman, G. J. (2006). Principles of helicopter aerodynamics with CD extra. Cambridge University press
[11] Padfield, G. D. (2008). Helicopter flight dynamics. Chichester, UK: John Wiley & Sons
[12] Hilbert, K. B. (1984). A mathematical model of the UH-60 helicopter. NASA TM 85890
[13] Okamoto, M., Nonaka, T., Ochiai, S., & Tominaga, D. (1998). Nonlinear numerical optimization with use of a hybrid genetic algorithm incorporating the modified Powell method. Applied Mathematics and Computation, 91(1), 63-72
[14] Yeo, H., Bousman, W. G., & Johnson, W. (2004). Performance analysis of a utility helicopter with standard and advanced rotors. Journal of the American Helicopter Society, 49(3), 250-270
[15] Roumeliotis I., Nikolaidis T., Pachidis V., Broca O., Unlu D., 2018, "Dynamic Simulation of a Rotorcraft Hybrid Engine in Amesim", 44th European Rotorcraft Forum, Delft, The Netherlands, 19-20 September, 2018
[16] Frosina, E., Senatore, A., Palumbo, L., Di Lorenzo, G., Pascarella, C., 2018, "Development of a Lumped Parameter Model for an Aeronautic Hybrid Electric Propulsion System", Aerospace 2018, 5(4), 105
[17] Hangiu Radu-Petru, Filip Andrei-Toader, Martis Claudia Steluta, Biró Károly Ágoston, "System-level Modeling and Simulation of a Permanent Magnet Synchronous Motor for an Integrated Starter Alternator". Journal of Electrical and Electronics Engineering, 5(2):67-70 (October 2012)
[18] Ed. Gunston B., 2004, "Jane's Aero-Engines", Issue Fifteen - March 2004, Jane's Information Group Limited
[19] Ballin M. G. A High Fidelity Real-Time Simulation of a Small Turboshaft Engine. Technical report, NASA Ames Research Center, 1988
[20] Gaudet S.R, Gauthier J. E. D., 2007, "A simple sub-idle component map extrapolation method", ASME paper No GT2007-27193
[21] Kurzke J., 2007, "About Simplifications in Gas Turbine Performance Calculations", ASME paper No. GT2007-27620, Proceedings of GT2007, ASME Turbo Expo 2007: Power for Land, Sea and Air, May 14-17, 2007, Montreal, Canada.
[22] Roumeliotis I., Aretakis N., Alexiou A., 2017, "Industrial Gas Turbine Health and Performance Assessment With Field Data", ASME J. Eng. Gas Turbines Power 139(5)
[23] Lolis, P., (2014), "Development of a Novel Preliminary Aero Engine Weight Estimation Method", PhD Thesis, Propulsion Engineering Centre, Cranfield University
[24] Carretero J. O., (2018), "Novel Turboshaft Engines Design and Optimisation for Rotorcraft Applications", PhD Thesis, Propulsion Engineering Centre, Cranfield University
[25] Vratny C. P., Forsbach F., Seitz A., Hornung M., 2014, "Investigation of Universally Electric Propulsion Systems for Transport Aircraft", 29th Congress of the International Council of the Aeronautical Sciences at: St. Petersburg, Russia
[26] Wintrich A., Nicolai U., Tursky W., Reimann T., 2015, "Power Semiconductors", Semikron, Semikron International GmBh, Verlag, 2015
[27] Nicolas Marc. Méthodologie de dimensionnement d'un véhicule hybride électrique sous contrainte de minimisation des émissions de CO2. Université d'Orléans, 2013.
[28] M. Petit, N. Marc, F. Badin, R. Mingant and V. Sauvant-Moynot, A Tool for Vehicle Electrical Storage System Sizing and Modelling for System Simulation, 2014 IEEE Vehicle Power and Propulsion Conference (VPPC), Coimbra, p. 91-96.
[29] Growatt CP250 datasheet, Segen, Growatt New Energy Technology Co., LTD

[30] Rucker J. E, 2005, “Design and Analysis of a Permanent Magnet Generator for Naval Applications”, MIT, Master of Science in Electrical Engineering and Computer Science, 2005
[31] Pyrhönen J., Jokinen T., Hrabovocá V., “Design of Rotating Electrical Machines”, 2nd edition, John Wiley&Sons, Ltd., 2008
[32] Lokhandwalla M., Haran K.S., Alexander J.P., “Scaling studies of High Speed High Temperature Superconducting Generator”, IEEE, 2012
[33] Carraro E, Degano M, Morandin M, Bianchi N., 2013, Formula SAE Electric Competition : Electrical Motor Design. Electric Machines & Drives Conference ,Chicago, pp 1142–1148, 2013
[34] Tsalavoutas A., Kelaidis M., Thoma N., Mathioudakis K. Correlations Adaptation for Optimal Emissions Prediction, ASME TURBO EXPO 2007 Proceedings, GT2007-27060. Montreal, Canada; 2007
[35] Celis, C., 2010 Evaluation and optimisation of environmentally friendly aircraft propulsion systems, Cranfield University, PhD Thesis, UK
[36] De Soete, G.G., 1975, January. Overall reaction rates of NO and N2 formation from fuel nitrogen. In Symposium (international) on combustion (Vol. 15, No. 1, pp. 1093-1102)
[37] Zeng Q, Liu Y., Sun X, Sethi, V., and Nalianda, D. Prediction of NOx for double annular combustors using stirred reactor approach. Proceeding of ISABE-22599, 2017
[38] Celis, C., Moss, B. and Pilidis, P., 2009, January. Emissions modelling for the optimization of greener aircraft operations. In ASME turbo expo 2009: power for land, sea, and air (pp. 167-178)
[39] Lefebvre A. H., Ballal D. R., “Gas Turbine Combustion: Alternative Fuels and Emissions”, 3rd Ed., Boca Raton FL: CRC Press, 2010, ISBN: 9781420086058
[40] Kyprianidis K. G., Nalianda D., Dahlquist E., “A NOx Emissions Correlation for Modern RQL Combustors”, The 7th International Conference on Applied Energy – ICAE2015, Energy Procedia 75 (2015) 2323 – 2330
[41] Green, J. (2002). Greener by Design — the technology challenge. The Aeronautical Journal (1968), 106(1056), 57-113. doi:10.1017/S0001924000095993
[42] Becker T., Perkavec M. A., “The Capability of Different Semianalytical Equations for Estimation of NOx Emissions of Gas Turbines”, ASME paper No. 94-GT-282, 1994
[43] Blazowski W.S., Walsh D.E., Mach K.D., “Operating and Ambient Condition Influences on Aircraft Gas Turbine NOx Emissions”, Journal of Aircraft, Vol. 12, No. 2 (1975), pp. 110-115
[44] Chandrasekaran N., Guha A., “Study of Prediction Methods for NOx Emission from Turbofan Engines”, Indian Institute of Technology Kharagpur, Pin 721 302, India, Journal of Propulsion and Power Vol. 28, No. 1, January–February 2012
[45] Tacina K. M., Lee C. M., Wey C., “NASA Glenn High Pressure Low NOx Emissions Research”, NASA/TM—2008-214974, February 2008
[46] Blazowski W.S., Walsh D.E., Mach K.D., “Operating and Ambient Condition Influences on Aircraft Gas Turbine NOx Emissions”, Journal of Aircraft, Vol. 12, No. 2 (1975), pp. 110-115
[47] Murthy J. N., “Gas Turbine Combustor Modelling for Design”, Cranfield University, PhD Thesis, 1988
[48] Mellor A. M., “Design of modern turbine combustors”, London: Academic Press, 1990
[49] Li J., XiaoXiao S., Yize L., Sethi V., 2017, “Preliminary Aerodynamic Design Methodology for Aero Engine Lean Direct Injection Combustors”, Aeronautical Journal, Vol 121, Issue 1242, August 2017, pp. 1087-1108
[50] Mattingly J. D., Heiser W. H., Pratt D. T., “Aircraft engine design”, 2nd edition, Reston, VA: American Institute of Aeronautics and Astronautics, ©2002, ISBN: 9781563475382
[51] Peter G. Bruce, Stefan A. Freunberger, Laurence J. Hardwick, Jean-Marie Tarascon, "Li-O2 and Li-S batteries with high energy storage", Nature Materials, 2011
[52] Gerald V. Brown, "Weights and Efficiencies of Electric Components of a Turboelectric Aircraft Propulsion System", NASA, 49° AIAA Aerospace Sciences Meeting, Orlando, 2011
[53] Johannes Brombach, Torben Schröter, Arno Lucken, Detlef Schulz, "Optimizing the Weight of an Aircraft Power Supply System through a +/- 270 VDC Main Voltage", Przeglad Elektrotechniczny, Helmut-Schmidt-University, Airbus Operations GmbH, 2012
[54] Anton F., “eAircraft: Hybrid-elektrische Antriebe für Luftfahrzeuge”,https://www.bbaa.de/fileadmin/user_upload/02-preis/02-02-preistraeger/newsletter-2019/02-2019-09/02_Siemens_Anton.pdf
[55] Xue N., Du W., Gupta A., Shyy W., Sastry A.M., Martins J.R.R.A., 2013, “Optimization of A Single Lithium-Ion Battery Cell With A Gradient-Based Algorithm”, J. Electrochem.
Soc. 160 (8) (2013) A1071–A1078
[56] International Energy Agency (IEA). Recent Trends in the OECD: Energy and CO2 Emissions; International Energy Agency (IEA): Paris, France, 2016

Performance and emission assessment of thermo-electric power plant for rotorcraft propulsion

Roumeliotis, Ioannis

2021-01-11

Roumeliotis I, Arena F, Liu Y, et al., (2021) Performance and emission assessment of thermo-electric power plant for rotorcraft propulsion. In: ASME Turbo Expo 2020: Turbomachinery Technical Conference and Exposition, 21-25 September 2020, London, Virtual Event. Paper number GT2020-15724

https://doi.org/10.1115/GT2020-15724